J Physiol 587.11 (2009) pp 2487–2497

The Journal of Physiology

Ether-à-go-go-related gene K^+ channels contribute to threshold excitability of mouse auditory brainstem neurons

Rachael M. Hardman and Ian D. Forsythe

MRC Toxicology Unit, University of Leicester, Leicester LE1 9HN, UK

The ionic basis of excitability requires identification and characterisation of expressed channels and their specific roles in native neurons. We have exploited principal neurons of the medial nucleus of the trapezoid body (MNTB) as a model system for examining voltage-gated K^+ channels, because of their known function and simple morphology. Here we show that channels of the *ether-à-go-go*-related gene family (ERG, Kv11; encoded by *kcnh*) complement Kv1 channels in regulating neuronal excitability around threshold voltages. Using whole-cell patch clamp from brainstem slices, the selective ERG antagonist E-4031 reduced action potential (AP) threshold and increased firing on depolarisation. In P12 mice, under voltage-clamp with elevated $[K^+]_o$ (20 mM), a slowly deactivating current was blocked by E-4031 or terfenadine ($V_{0.5,act} = -58.4 \pm 0.9$ mV, $V_{0.5,inact} = -76.1 \pm 3.6$ mV). Deactivation followed a double exponential time course ($\tau_{slow} = 113.8 \pm 6.9$ ms, $\tau_{fast} = 33.2 \pm 3.8$ ms at -110 mV, τ_{fast} 46% peak amplitude). In P25 mice, deactivation was best fitted by a single exponential ($\tau_{fast} = 46.8 \pm 5.8$ ms at -110 mV). Quantitative RT-PCR showed that ERG1 and ERG3 were the predominant mRNAs and immunohistochemistry showed expression as somatic plasma membrane puncta on principal neurons. We conclude that ERG currents complement Kv1 currents in limiting AP firing at around threshold; ERG may have a particular role during periods of high activity when $[K^+]_o$ is elevated. These ERG currents suggest a potential link between auditory hyperexcitability and acoustic startle triggering of cardiac events in familial LQT2.

(Received 6 February 2009; accepted after revision 31 March 2009; first published online 9 April 2009)
Corresponding author I. D. Forsythe: MRC Toxicology Unit, University of Leicester, Leicester LE1 9HN, UK.
Email: idf@le.ac.uk

Abbreviations AP, action potential; AHP, after hyperpolarisation; DTx-I, dendrotoxin-I; ERG, *ether-à-go-go*-related gene; I_H, hyperpolarisation activated non-specific cation current; I_{Kr}, cardiac delayed rectifier K^+ current; Kv, voltage-gated K^+ channel; LSO, lateral superior olive; MNTB, medial nucleus of the trapezoid body; MSO, medial superior olive; NaV, voltage-gated Na^+ channel; QRT-PCR, quantitative real time polymerase chain reaction; $V_{0.5,act}$, membrane potential at half-maximal activation; $V_{0.5,inact}$, membrane potential at half-maximal inactivation; V_m, test potential.

The medial nucleus of the trapezoid body (MNTB) serves as an inverting relay in circuits involved in sound-source localisation, converting excitatory inputs from the contralateral cochlear nucleus bushy cells into inhibitory responses for the ipsilateral medial and lateral superior olives (MSO and LSO, respectively) (Cant & Casseday, 1986; Smith *et al.* 1991, 1998; Henkel & Gabriele, 1999). The MNTB principal neurons receive the giant calyx of Held synapse (Schneggenburger & Forsythe 2006), which generates a large EPSC by activation of AMPA glutamate receptors with unusually rapid kinetics (Taschenberger & von Gersdorff, 2000; Joshi & Wang, 2002; Postlethwaite *et al.* 2007). This large magnitude EPSC helps preserve timing information, but the large conductance requires precise and powerful control of postsynaptic excitability through expression of a suite of K^+ conductances, predominantly mediated by voltage-gated channels from families Kv1–Kv4. Each family has a particular role in regulating postsynaptic excitability. Kv1 channels suppress excitability around AP threshold, so that the principal neuron faithfully follows the pattern and timing of the calyceal input (Brew & Forsythe, 1995; Dodson *et al.* 2002; Gittelman & Tempel, 2006). Kv2.2 channels regulate the inter-spike voltage (Johnston *et al.* 2008*b*) during high frequency firing, assisting recovery of sodium channels from inactivation and thereby maintaining the MNTB AP during repetitive activity. Channels containing Kv3 have high threshold and fast kinetics, enhancing rapid

DOI: 10.1113/jphysiol.2009.170548

repolarisation, giving short duration APs and promoting high-frequency firing (Brew & Forsythe, 1995; Wang *et al.* 1998). There is also a small contribution from Kv4 (Johnston *et al.* 2008*a*), which acts to accelerate the initial AP time course during repetitive firing. Although these four families contribute the majority of outward potassium currents, other families may also make important contributions.

Ether-à-go-go-related gene (ERG, Kv11) channels are voltage-gated K^+ channels with unusual kinetics, in that their inactivation rates vastly exceed activation rates, so that the greatest conductance is generated on repolarisation rather than depolarisation (Mitcheson & Sanguinetti, 1999). Three genes (*kcnh2*, *-6* and *-7*) have been identified in mammals. ERG1 (encoded by *kcnh2*) is extensively studied, being responsible for the cardiac delayed rectifier current I_{Kr} (Sanguinetti & Tristani-Firouzi, 2006). The broader therapeutic implication is that ERG1 block by a wide variety of medications (or loss of function due to inherited mutations) causes cardiac arrhythmias (LQT syndrome) and sudden death (Sanguinetti & Tristani-Firouzi, 2006). All three ERG genes are expressed in the brain (Shi *et al.* 1997; Guasti *et al.* 2005) but their role(s) in the nervous system is unclear.

In this study, we combine electrophysiological, pharmacological, QRT-PCR and immunohistochemical evidence to demonstrate that ERG currents are present in mouse MNTB principal neurons and show that they act at voltages around firing threshold to suppress excitability and complement low-voltage-activated Kv1 conductances.

Methods

Slice preparation

Brainstem slices were prepared as previously described (Dodson *et al.* 2002; Johnston *et al.* 2008*b*). Briefly, 11- to 14-day-old or 25- to 28-day-old CBA/Ca mice were killed by decapitation (in accordance with the UK Animals Scientific Procedures Act, 1986). In some cases (as noted in the text) recordings were made from brain slices obtained from 11- to 14-day-old Lister Hooded or Wistar rats using identical methods. These ages were selected because rodent hearing onset is around P11, but further developmental change in ion channel expression is possible, and so after weaning the age-group P25–28 was also studied. The brain was excised in ice-cold low-Na^+ artificial cerebrospinal fluid (aCSF), containing (in mM): KCl (2.5), glucose (10), NaH_2PO_4 (1.25), $NaHCO_3$ (26), $CaCl_2$ (0.1), $MgCl_2$ (4), ascorbate (0.5) and sucrose (250); gassed with 95% O_2–5% CO_2 giving pH 7.4. Slices were cut (200 μm thick) using an IntegraSlice (Campden Instruments) and maintained at 37°C for 1 h in gassed aCSF containing (in mM): NaCl (125), KCl (2.5), glucose (10), ascorbate (0.5) NaH_2PO_4 (1.25), $NaHCO_3$ (26), sodium pyruvate (2), *myo*-inositol (3), $CaCl_2$ (2), $MgCl_2$ (1), pH 7.4. The slices were then allowed to cool to room temperature. Chemicals and reagents were purchased from Sigma, (Poole, UK) unless otherwise noted.

Electrophysiology

One slice was placed in an environmental chamber on a Nikon FN600 microscope stage and continuously perfused with gassed (95% O_2–5% CO_2) aCSF at a rate of 1 ml min^{-1} at room temperature. Whole-cell recordings were made from visually identified MNTB neurons using an Axopatch 200B amplifier (Molecular Devices, Union City, CA, USA). Patch solution comprised (in mM) potassium gluconate (97.5), KCl (32.5), Hepes (10), EGTA (5), $MgCl_2$ (1), pH 7.2 with KOH. The I_H channel blocker ZD-7288 (0.01 mM, Tocris Cookson, Bristol, UK) was routinely included in the patch solution. Pipettes had resistances of 3–5 MΩ and series resistances were 6–10 MΩ (compensated by 70%, 10 μs lag). Access resistance was frequently monitored and the recording discarded if increases were more than 2 MΩ.

ERG currents were identified under voltage clamp using a high $[K^+]_o$ (20 mM, substituted for $[Na^+]_o$) and low $[Ca^{2+}]_o$ (0.5 mM, replaced with $MgCl_2$) solution. One millimolar tetraethylammonium (TEA), 1 μM tetrodotoxin (TTX, Laxotan, Valence, France), 10 nM dendrotoxin-I (DTX-I, Alomone Laboratories, Jerusalem, Israel), 5 mM kynurenic acid, 10 μM bicuculline (Tocris) and 1 μM strychnine were added to block Kv3, NaV, Kv1, glutamate receptors, $GABA_A$ and glycine receptors, respectively. Where noted, E-4031 (*N*-[4-[[1-[2-(6-methyl-2-pyridinyl)ethyl]-4-piperidinyl] carbonyl]phenyl]methanesulfonamide dihydrochloride) or terfenadine (α-[4-(1,1-Dimethylethyl)phenyl]-4-(hydroxydiphenylmethyl)-1-piperidinebutanol; a gift from Dr J. Mitcheson, University of Leicester) was either included in the patch pipette (1 μM) or extracellularly perfused (10 μM).

Quantitative RT-PCR

RNA extraction was carried out on P12 and P25 CBA mice using TRI reagent and DNAse treated. RT-PCR for mouse ERG and Kv3.1b transcripts was performed on 2 μg of RNA sample using the SuperScript III first strand synthesis kit and oligo-dT primers (Invitrogen, Paisley, UK). Primer sequences were as follows.

mERG1 – fwd: GATCGCCTTCTACCGGAAA, rev: CATTCTTCACGGGTACCACA,
mERG2 – fwd: ATGCTTCTGGTGGGACATCT, rev: GAGGTATCCTGGGGGAGAAA,

mERG3 – fwd: AGACGGAAAGCGACCTCAC, rev: CGTTGTCATTTGGGATTCAA,
Kv3.1b – fwd: TCTGCAAAGCCTACGGATTC, rev: AGGCTCAGCAAGGCTAAGG.

Amplification was achieved using the following conditions: 50°C 2 min, 95°C 10 min, followed by 95°C 15 s and 60°C 60 s for 40 cycles. Primer efficiency was >95%. Relative expression levels were assessed using the comparative C_T method (User Bulletin 2, ABI Prism Sequence Detection System, pp. 11–15, 1997, PE Applied Biosystems), with $\Delta\Delta C_T$ values for ERG normalised to $\Delta\Delta C_T$ values for Kv3.1b.

Immunohistochemistry

P12 and P25 CBA mice brainstems were isolated without fixation and frozen in Tissue Tek (Sakura Finetek, Zoeterwoude, NL), using hexane and dry ice. Cryostat sections of 12 μm were cut, mounted on polylysine-coated slides and fixed. Since tissue was sectioned before fixation, favourable antibodies were put through a fixation 'matrix' of four conditions (paraformaldehyde (PFA), 4%; PFA with antigen retrieval, methanol, or no fixation). For each antibody used, the most favourable fixing condition was 100% methanol at −20°C for 5 min. Following 3 × 5 min washes in 100 mM phosphate-buffered saline (PBS) with 0.1% Triton-X100 (PBS-T), sections were blocked for 1 h at 20°C in 1% bovine serum albumin (BSA), 1% goat serum PBS-T (blocking buffer). Sections were incubated at 4°C overnight in blocking buffer containing the appropriate ERG and Kv3.1b primary antibodies. Commercial primary antibodies were initially considered from Western blots displaying either blocking peptide or knock-out animal controls. Anti-ERG1 (Alomone, APC-016) was rejected due to non-specific staining in the presence of blocking peptide (data not shown). The antibodies used were anti-ERG1 (seq: RQRKRKLSFRRRTDKDTEQ, a kind gift from Gail Robertson, 1:500, validated by Western blot, see Roti *et al.* 2002), anti-ERG2 (seq: TLNFVEFNLEKHRS(C), Alomone, 1:2000), anti-ERG3 (seq: CPEFLDLEKSKLKSKE, Alomone, 1:2000) and anti-Kv3.1b (NeuroMab, 1:1000, no sequence but validated by Western blot and knockout mice showing no staining).

After 3 × 10 min washes, secondary antibodies (goat anti-rabbit Alexa-fluor 488 (1:1000) and goat anti-mouse Alexa-fluor 546 (1:500), Molecular Probes, Paisley, UK), were applied for 2 h at 20°C. Sections were then subjected to a further 3 × 10 min washes in PBS-T before being mounted with Vectashield containing DAPI (Vector Labs, Peterborough, UK). Images were taken using a conventional Leica fluorescence microscope (DM2500) fitted with a charge coupled device (CCD) camera (DFC350Fx) or a Zeiss LSM 510 Meta confocal microscope. Control sections underwent identical procedures, but were pre-incubated with immunizing peptide ('blocking peptide') for at least 1 h at room temperature.

Voltage protocols and data analysis

Data was acquired using pCLAMP 9.2 with a Digidata 1322A interface (Molecular Devices), filtered at 2–5 kHz and digitized at 20–50 kHz. A holding potential of −80 mV (after correction for a liquid junction potential of 10 mV) was used, whilst neurons under current clamp were held at −70 to −80 mV. Details of protocols are provided in the figure legends and Results.

Analysis of the voltage dependence of activation and the kinetics of deactivation were performed using Clampfit 9 software (Molecular Devices). Activation parameters were determined using the Boltzmann function:

$$I(V) = 1/(1 + \exp(V_{0.5,\mathrm{act}} - V_\mathrm{m})/k$$

Where $I(V)$ is normalised current, V_m is the test potential, $V_{0.5,\mathrm{act}}$ is the mid-point and k the slope factor for activation.

To determine the rate of deactivation, the decay phase of tail currents were fit with either a single or double exponential of the forms:

$$I(t) = A\exp(t/\tau) + C$$

or

$$I(\tau) = A_\mathrm{fast}\exp(t/\tau_\mathrm{fast}) + A_\mathrm{slow}\exp(t/\tau_\mathrm{slow}) + C$$

where τ refers to the time constant of deactivation, A is the amplitude of each component and C is a constant.

Data are presented as means ± S.E.M. (N = number of animals, n = number of cells) with statistical analysis using unpaired, Student's two-tailed t-test, one way ANOVA with Bonferroni's correction or two-way ANOVA.

Results

E-4031 increases AP firing in MNTB neurons

Whole cell patch recordings were made from MNTB neurons of P11–P14 mice under current clamp. In control conditions, from a membrane potential of −70 mV (Fig. 1*A*), single APs were evoked by current injections greater than 150 pA, ($N = 3$, $n = 4$). Inclusion of the ERG antagonist E-4031 (1 μM) in the pipette solution did not alter the resting membrane potential but reduced the threshold to 100 pA ($N = 3$, $n = 4$, Fig. 2*A*) and also increased mean AP firing from 1.25 ± 0.25 to 16.5 ± 3.75 spikes in response to 200 ms, 200 pA current injection (Fig. 2*B*). At 600 pA (Fig. 1*B*) firing increased to 28.25 ± 5.84 APs ($N = 3$, $n = 4$). E-4031 had no effect on AP half-width (Fig. 2*C*), amplitude or latency (data not

shown). E-4031 effects under current clamp were similar to block of Kv1 channels (Dodson *et al.* 2002), raising the possibility of non-specific block. However this was not the case since control experiments showed that DTx-I (10 nM) further increased AP number (data not shown) while ERG currents measured under voltage-clamp were DTx-I resistant (see Figs 5 and 6). When identical experiments were conducted from P11–P14 Lister Hooded or Wistar rats, E-4031 caused no alteration to threshold or firing rate ($N = 3$, $n = 3$, Fig. 3*A* and *B*) and under voltage clamp there was no measurable ERG current (Fig. 3*C*), suggesting an interesting species difference in that ERG channels do not contribute to excitability in rat MNTB neurons at this stage of development.

MNTB neurons express an ERG-like current

It proved hard to measure ERG currents with 2.5 mM $[K^+]_o$ aCSF (data not shown). Increasing $[K^+]_o$ and reducing $[Ca^{2+}]_o$ increases ERG current in cell lines (Johnson *et al.* 2001; Sturm *et al.* 2005) and a similar approach using aCSF containing 20 mM $[K^+]_o$ and 0.5 mM $[Ca^{2+}]_o$ was applied here to measure ERG currents in the MNTB. Tail currents were measured under voltage-clamp at −110 mV after a 5 s depolarising pulse to −20 mV (from a holding potential of −80 mV). Extracellular perfusion of E-4031 (10 μM) blocked tail currents by $65.31 \pm 9.4\%$ ($N = 3$, $n = 4$, Fig. 4) whilst terfenadine (10 μM) blocked them by $54.76 \pm 2.1\%$ ($N = 2$, $n = 3$, Fig. 4). P25 mice displayed a significantly larger ERG current than P12 mice. Using the same depolarising step protocol, a peak tail amplitude of -0.48 ± 0.09 nA was obtained for P25 mice compared to -0.26 ± 0.03 nA for P12 mice ($N = 3$, $n = 3$, Student's unpaired t-test $P < 0.05$).

The voltage dependence of activation was determined using 5 s depolarising pulses between −90 and −10 mV, applied from a holding potential of −80 mV and with tail currents measured at −110 mV (Fig. 5*D*). The ERG current (Fig. 5*Ac* and *Bc*) was obtained by subtraction of the current resistant to E-4031 (Fig. 5*Ab* and *Bb*) from control traces (Fig. 5*Aa* and *Ba*). Activation of currents was detected at −70 mV (Fig. 5*C*). The activation curve was constructed by plotting the normalised peak amplitude of tail currents against the voltage step potential. Fitting with a Boltzmann function gave a $V_{0.5,act}$ of −58.13 mV with a slope factor of 3.28 for P12 animals. P25 animals displayed a small shift in $V_{0.5,act}$ to −56.50 mV and had a significant shift in the slope value to 8.61 (Fig. 5*C* and Table 1). The tail current remaining after E-4031 block had a $V_{0.5,act}$ of around −15 mV (data not shown), similar to that previously shown for Kv2.2 (Johnston *et al.* 2008*b*).

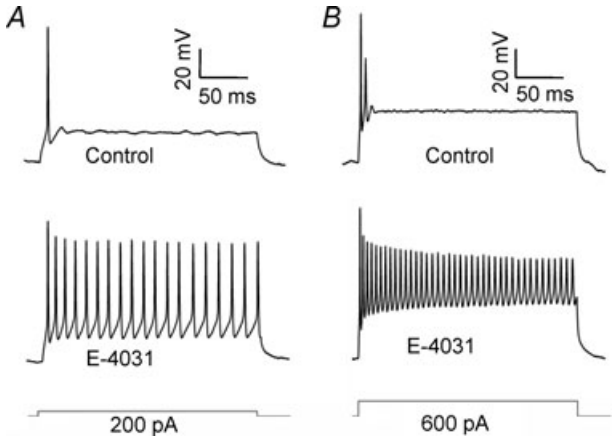

Figure 1. Suppression of ERG currents increases MNTB excitability
Current clamp recordings from MNTB neurons on injection of depolarising current show the phenotypic one or two initial action potentials on depolarising current injection: 200 pA (*A*) and 600 pA (*B*) in control (2.5 mM K^+) aCSF (top). Addition of E-4031 (1 μM), included in the patch pipette (lower traces), caused a significant increase in neuronal firing in all cells tested. The current steps are shown below.

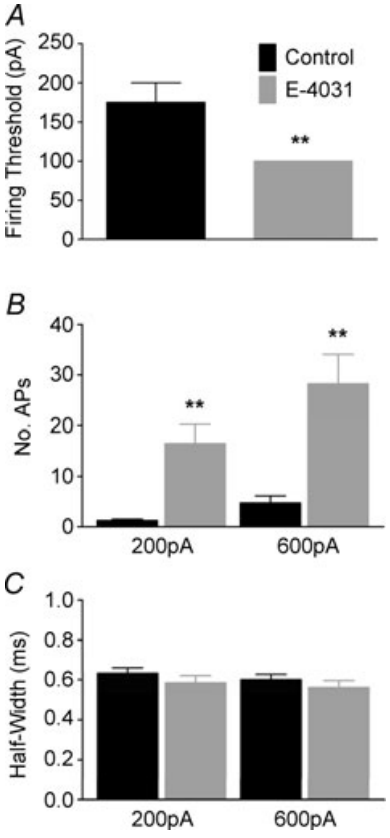

Figure 2. ERG channels raise AP threshold but have little influence on AP duration
Bar graphs showing the effects of E-4031 on the firing threshold (*A*), AP firing frequency on injection of 200 or 600 pA depolarising current (*B*) and AP half-width on injection of 200 or 600 pA current (*C*). E-4031 caused a significant increase in neuronal firing and a reduction in firing threshold without altering the AP waveform (Student's unpaired t-test, ** $P < 0.01$).

To study the voltage-dependency of *quasi* steady-state inactivation, the potential was stepped to −10 mV for 4 s, to activate and inactivate all channels, then stepped back to different potentials (−10 to −130 mV) to allow recovery from inactivation (Fig. 6*C*). Since ERG channels deactivate at the same potentials as they recover from inactivation, the decay of the tail currents were fitted by an exponential function with the amplitude extrapolated to the end of the depolarising voltage step (Fig. 6*C*). For P12 animals, fitting was best using a double exponential whilst for P25 mice, a single exponential was most appropriate (Fig. 6*D*), although there was a small component that could not be fitted, reflecting a small additional conductance. The chord conductance was calculated by dividing the extrapolated current by the driving force and normalising to the maximum chord conductance (Fig. 6*E*). The data points were fitted with a Boltzmann function, giving a $V_{0.5,\text{inact}}$ of −76.0 mV and a slope of 17.7 for P12 mice ($N = 3$, $n = 4$). P25 mice had a $V_{0.5,\text{inact}}$ of −70.8 mV and a slope of 14.7 ($N = 3$, $n = 3$), similar to the results for P12 animals.

The same protocol also gave time constants of deactivation (Fig. 6*F* and *G* and Table 1). For P12 animals, at negative potentials (−130 to −110 mV), the deactivation followed a double exponential function, with clear voltage dependency for both time constants (Fig. 6*F*,*G*. $N = 3$, $n = 4$). The slow time constant was not measurable in the P25 age group, due to additional noise at negative voltages. At less negative potentials (−100 to −80 mV), deactivation was fitted by a single exponential function for P12 and P25 animals. Deactivation became faster with membrane hyperpolarisation; with the mean τ_{fast} accelerating from 151.8 ms at −80 mV to 15.2 ms at −130 mV, and τ_{slow} from 141.2 ms at −110 mV to 41.3 ms at −130 mV (Fig. 6*F* and *G*). As for P12 mice, the rate of deactivation for P25 mice increased with membrane hyperpolarisation, with the mean τ_{fast} reducing from 162.1 ms at −80 mV to 21.1 ms at −130 mV. There was a slight but statistically insignificant increase of all time constants for P25 compared to P12 animals except at potentials positive to −100 mV, where a significant increase in the rate of deactivation was observed (Fig. 6*G* and Table 1).

ERG mRNA and protein is present in the MNTB

QRT-PCR was performed on superior olivery complex (SOC) tissue dissected from the brainstem, to determine which ERG transcripts are present. Comparison against Kv3.1b levels (in the same brain region) from P12 showed high levels of mRNA for ERG1 and ERG3, whilst ERG2 showed significantly less expression ($N = 3$, Fig. 7*A*). A similar result was seen for P25 mice ($N = 3$, Fig. 8*A*). Relative expression levels were similar between P12 and P25 animals although ERG3 showed a significant reduction in expression levels in P25 animals (one-way ANOVA, $P < 0.05$).

The protein expression and distribution of ERG subunits was examined using subtype-specific antibodies and co-labelling with anti-Kv3.1b to confirm identification of MNTB principal neurons (Wang *et al.* 1998; Steinert *et al.* 2008). Consistent with the QRT-PCR data, strong staining was seen using conventional fluorescence

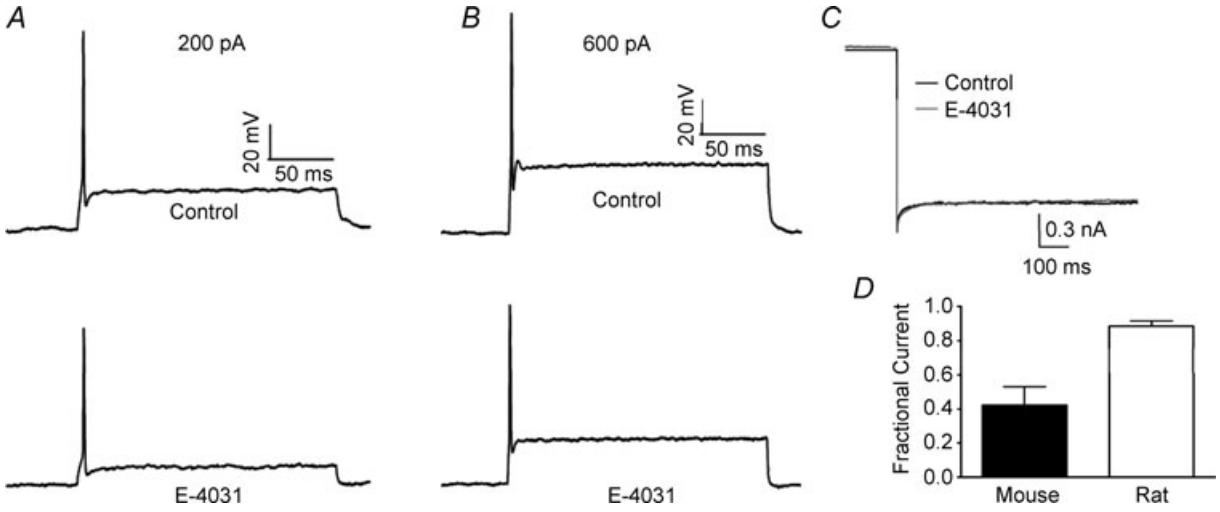

Figure 3. Rat MNTB neurons do not have an ERG-like current
A and *B*, current clamp recordings from MNTB neurons on injection of depolarising current at 200 pA (*A*) and 600 pA (*B*) under control conditions (top) and in the presence of E-4031 (bottom). E-4031 had no effect on neuronal firing. *C*, tail current recorded at −110 mV from a depolarising pulse of −10 mV in the presence (grey) and absence (black) of E-4031 (10 μM). *D*, fraction of current remaining after block by E-4031. E-4031 inhibited murine tail currents by over 50% whilst rat tail currents were inhibited by less than 12%.

Table 1. Biophysical properties of ERG channels in MNTB

Voltage dependence					
	$V_{0.5}$ (mV)	S.E.M.	Slope	S.E.M.	*n*
P12 Activation	−58.37	0.91	3.48	0.91	4
P12 Inactivation	−76.12	3.58	17.70	4.26	4
P25 Activation	−56.50	2.08	8.61*	1.98	4
P25 Inactivation	−70.77	2.77	14.71	2.87	3

Deactivation kinetics						
	P12			P25		
Voltage (mV)	τ_{fast} (ms)	S.E.M.	*n*	τ_{fast} (ms)	S.E.M.	*n*
−130	15.23	2.62	4	21.05	3.83	3
−110	33.15	3.84	4	46.78	5.77	3
−90	99.60	9.06	4	162.13**	2.11	3

Values are means ± S.E.M. *n* = number of cells. Statistical comparison of P12 and P25 data was performed using Student's *t*-test on voltage dependence (*$P < 0.05$) and two way ANOVA for deactivation kinetics (**$P < 0.01$).

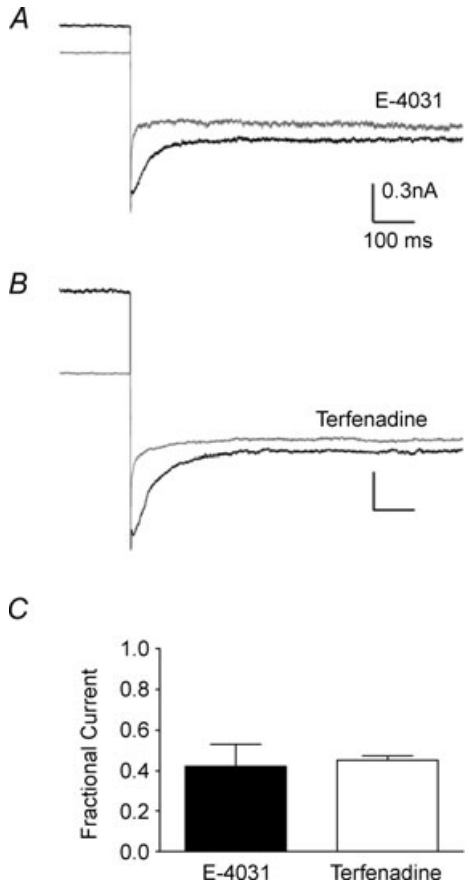

Figure 4. MNTB ERG currents are blocked by E-4031 and terfenadine
A and *B*, tail currents recorded at −110 mV after a −20 mV depolarizing pulse in the presence (grey) or absence (black) of E-4031 (10 μM) (*A*) or terfenadine (10 μM) (*B*) applied by extracellular perfusion in the aCSF. Plot of the fractional current remaining after antagonist perfusion (*C*). Both antagonists blocked a similar fraction of current and inhibited ERG current by over 50%.

microscopy for ERG1 (Fig. 7*C*) and ERG3 (Fig. 7*D*), whilst ERG2 staining was weak (Fig. 7*B*) with little staining above background. For each of the antibodies used, no staining was observed in the presence of the respective blocking peptides (Fig. 7*B–D*, insets). Using confocal microscopy, strong staining for ERG1 and ERG3 was seen in Kv3.1 positive principal neurons (Fig. 7*E* and *F*). Specific co-localisation with Kv3.1 was not apparent, although some overlap in staining was evident simply because these are channels in the cell membrane. There was clear evidence of punctate somatic membrane staining for both ERG channels (Fig. 7*Ga* and *Ha*, arrowheads), which is distinct from that seen for any other voltage-gated ion channel in the MNTB. There was

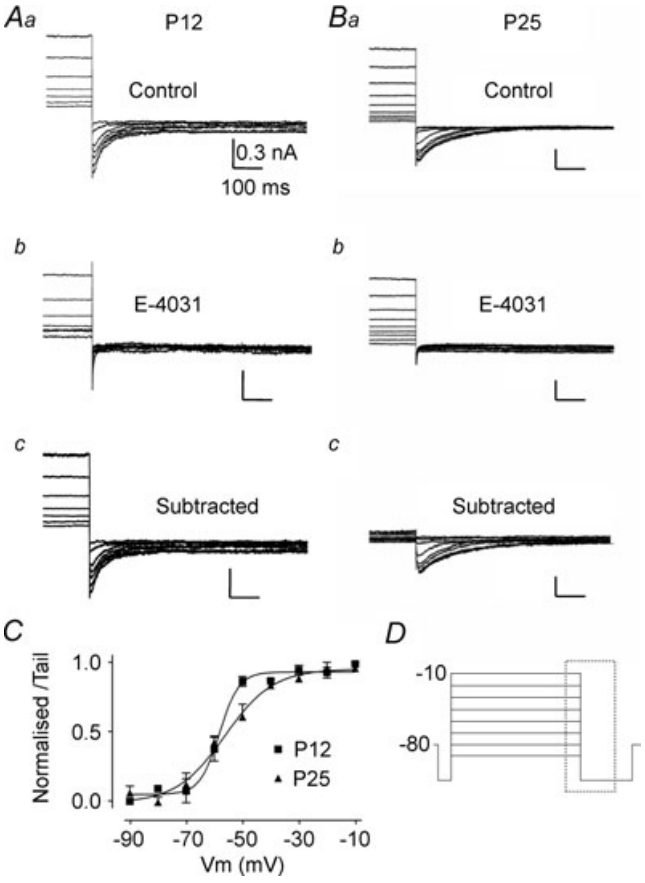

Figure 5. A fast ERG current is activated on depolarisation of MNTB neurons from P12 and P25 mice
A, data from P12. *B*, data from P25. For both ages superimposed currents are: control (*a*); following perfusion of E-4031 (*b*); and difference current observed by subtraction of *a* – *b* (c). All tail currents shown on stepping to −110 mV are activated by prior depolarising voltage steps with high K^+ aCSF (20 mM $[K^+]_o$, 0.5 mM $[Ca^{2+}]_o$). *C*, average normalized activation curves for E-4031-sensitive tail currents. Data were fitted with a Boltzmann function giving a $V_{0.5,act}$ of −58.13 ± 1.56 mV with a slope factor of 3.28 ± 0.5 for P12 and a $V_{0.5,act}$ of −56.50 ± 2.08 mV and slope of 8.61 ± 1.98 for P25 animals. *D*, voltage protocol for *A* and *B*; displayed currents occur within the dashed box. All scale bars correspond to values in *Aa*.

some punctate staining in the nucleus for ERG1 (Fig. 7*G*) which was blocked by blocking peptide, but we have no evidence for a nuclear specific function. As expected there was some cytoplasmic staining, particularly for ERG1 (Fig. 7*Ga*) and both ERG subtypes may be present in the initial segment (Fig. 7*Gb* and *Hd*, arrowheads). A similar pattern of staining was observed for P25 animals (Fig. 8), with punctate membrane staining being observed for ERG1 (Fig. 8*B*) and ERG3 (Fig. 8*D*).

Discussion

It is now possible to ascribe more specific functions to currents mediated by native Kv channel families

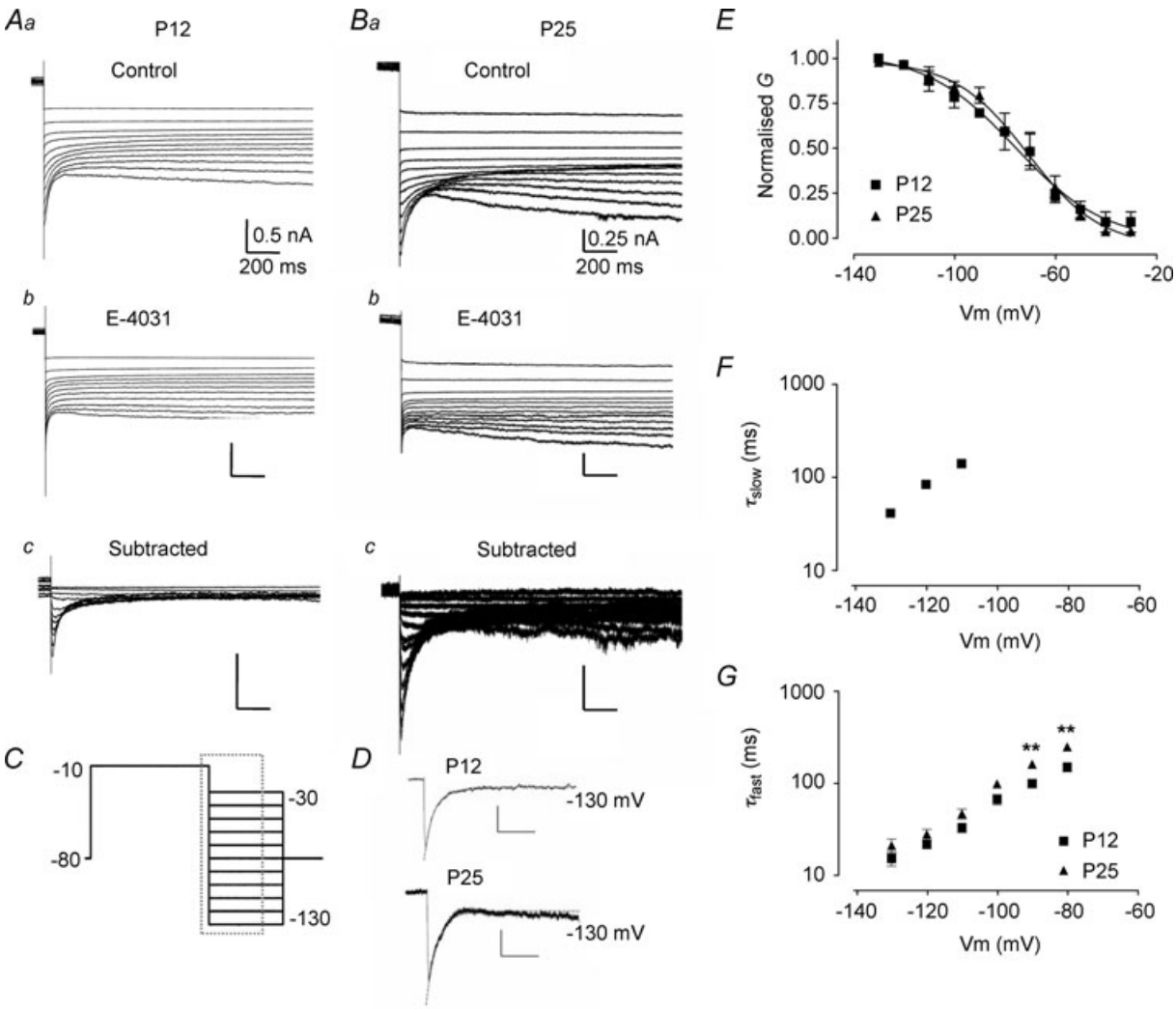

Figure 6. Deactivation of ERG currents from P12 and P25 mice
A, data from P12. *B*, data from P25. For both ages superimposed currents are: control (*a*); following perfusion of E-4031 (*b*); and difference current observed by subtraction of *a* – *b* currents at each voltage (*c*). All tail currents are shown following prior depolarising voltage steps to −10 mV with high K^+ aCSF (20 mM $[K^+]_o$, 0.5 mM $[Ca^{2+}]_o$). *C*, voltage protocol for *A* and *B*; displayed currents occur within the dashed box. Scale bars for *A* correspond to values in *Aa*, and for *B* to *Ba*. *D*, exponential fits for current decay at −130 mV for P12 and P25 mice. A double exponential was required to fit P12 data whilst P25 data was best fitted by a single exponential. *E*, quasi steady-state inactivation curves constructed from chord conductances normalised to the peak chord conductance. Boltzmann function fits gave a $V_{0.5,inact}$ of −76.12 ± 3.58 mV with a slope factor of 17.70 ± 4.26 for P12 and a $V_{0.5,inact}$ of −70.77 ± 2.77 mV and slope of 14.71 ± 2.87 for P25 animals. *F* and *G*, semi-logarithmic plots of deactivation time constants. For P12 mice, decay currents between −130 and −110 mV were fitted with a double exponential whilst a single exponential function was used between −100 and −80 mV. Currents recorded from P25 animals were fitted with a single exponential at all voltages and displayed significantly slower deactivation rates at −90 and −80 mV compared to P12 animals (2-way ANOVA, $^{**}P < 0.01$).

in identified neurons and so better understand their physiological significance. Here we show that the classical voltage-gated (Kv1–4) families present in MNTB neurons are complemented by expression of ERG channels, which act in synergy with Kv1 to reduce excitability at around threshold voltages. Our molecular and immunohistochemical data are consistent with heteromeric channels containing ERG1 and ERG3 subunits. Although well studied in the cardiovascular system, their physiological role in the CNS is only just beginning to be addressed.

Biophysical properties of the ERG current

Activation of MNTB ERG channels ($V_{0.5} = -58$ mV, $k = 3.3$) occurs at more negative voltages and with a steeper voltage dependence than in Purkinje neurons which also express both ERG1 and ERG3 (Sacco *et al.* 2003, $V_{0.5} = -50.7$ mV, $k = 5.6$) and mouse smooth muscle cells ($V_{0.5} = -51$ mV), which express ERG1 (Ohya *et al.* 2002). Recombinant rat ERG expressed in CHO cells showed negative shifts in $V_{0.5,act}$ with increasing extracellular potassium for ERG1 and ERG3 but was unchanged for ERG2 (Sturm *et al.* 2005). ERG3 exhibits a steeper slope (from 8.5 to 6.2) and faster deactivation kinetics with increasing $[K^+]_o$, so the fast deactivation kinetics of MNTB ERG tail currents are consistent with ERG3 dominated channels, while ERG1 homomeric channels display much slower deactivation (Sturm *et al.* 2005).

These data are consistent with ERG3 being a dominant contributor to the ERG current in MNTB neurons. However, steady-state inactivation values ($V_{0.5}$ of -72 mV and a slope of 21) were more negative than reported for ERG3 (Zou *et al.* 1998; Sturm *et al.* 2005) but similar

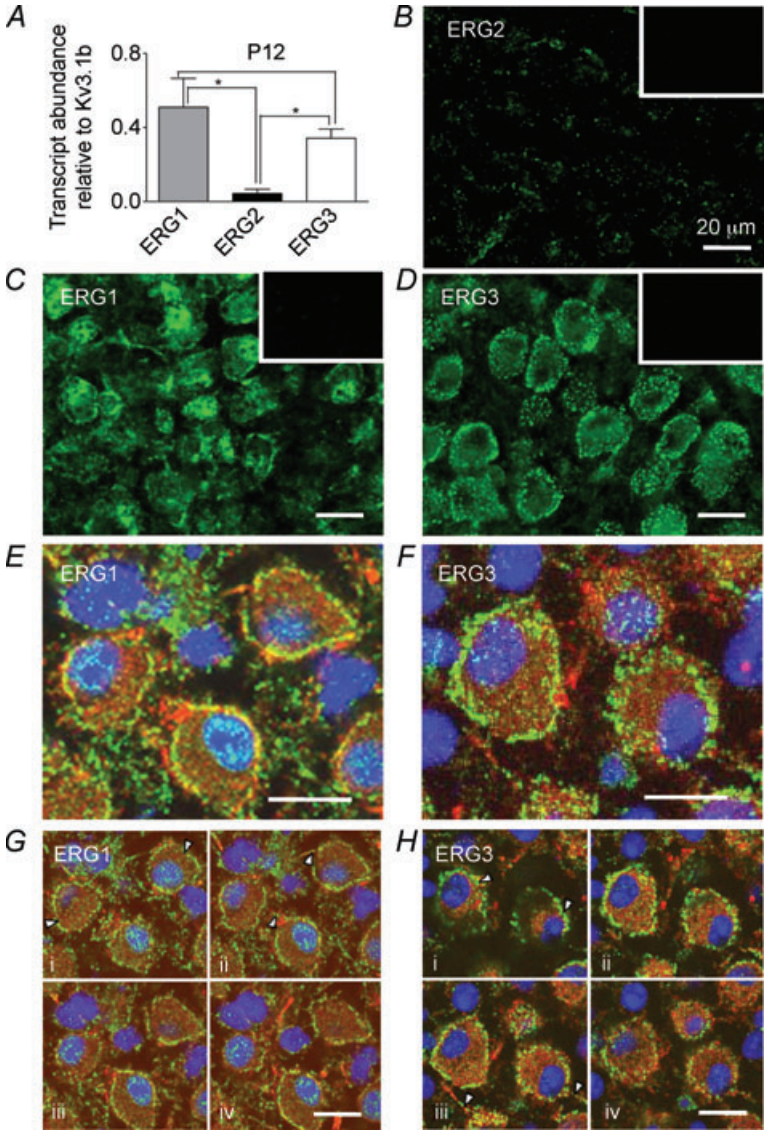

Figure 7. Immunohistochemistry shows both ERG1 and ERG3 are present in MNTB from P12 mice
A, QRT-PCR of ERG1, 2 and 3 mRNA expressed relative to Kv3.1b from P12 mice ($N = 3$, $n = 3$). ERG1 and ERG3 were present at significantly higher levels than ERG2 (one-way ANOVA with Bonferroni's correction, $^*P < 0.05$). *B–D*, fluorescence images showing ERG1, 2 and 3 antibody staining. *B*, ERG2 shows low staining levels. ERG1 (*C*) and ERG3 (*D*) immunoreactivity was high in the MNTB principal neurons. Insets show corresponding blocking peptide controls. *E* and *F*, confocal projections for ERG1 (green) (*E*) and ERG3 (green) co-labelled with Kv3.1b (red) and DAPI (blue) (*F*). *G* and *H*, four single optical z sections taken at 1 μm intervals through the same cells shown in *E* and *F*. Note the clear punctate membrane staining for both isoforms (arrowheads, *Ga* and *Ha*) and axon staining (arrowheads *Gb* and *Hc*). Scale bar (20 μm) applies to all panels.

to cerebellar Purkinje neurons (Sacco *et al.* 2003). Such minor discrepancies are common when comparing data from recombinant with native channels and could reflect heteromultimeric channels, an unidentified accessory subunit or endogenous phosphorylation/signalling activity.

Expression of ERG channel isoforms in MNTB neurons

QRT-PCR of the MNTB identified the transcripts for all three ERG isoforms (ERG1 > ERG3 >> ERG2), consistent with RNase protection assays where all isoforms of ERG are expressed in the adult murine central nervous system (Guasti *et al.* 2005). The QRT-PCR and immunohistochemical labelling were both conducted by reference to Kv3.1b, which is highly expressed in MNTB principal neurons (Wang *et al.* 1998; Dodson *et al.* 2003; Steinert *et al.* 2008). Both methods showed that ERG2 was present at lower levels than ERG1 and ERG3, and the expressed protein was present in neuronal plasma membranes, as expected for a functional ion channel. Unfortunately we were unable to test for ERG subunit co-localisation because the antibodies used were all raised in the same host species and so co-localization studies were not possible. ERG1 staining was also seen in the nuclear compartment; it is unclear whether this reflects some non-specific staining or whether it acts as a nuclear K^+ channel contributing to the K^+ permeability of the nuclear envelope (Bustamante, 2006). ERG channels have been implicated in cellular regulation at the nuclear level; ERG1 is known to play a role in H_2O_2-induced apoptosis (Han *et al.* 2004) and ERG1a and 1b protein expression is strongly cell-cycle dependent in tumour cells (Crociani *et al.* 2003).

A physiological role for ERG channels in the MNTB

There are relatively few physiological studies of ERG currents in the brain. In the heart, ERG1 has been identified as the pore-forming subunit for the cardiac delayed rectifier current I_{Kr} (Sanguinetti *et al.* 1995), where it contributes to the later stages of cardiac action potential repolarisation (Hancox *et al.* 1998).

Recent evidence demonstrates activity-dependent increases in ERG channel expression in vomeronasal sensory neurons (Hagendorf *et al.* 2009). ERG plays a role in slow AHPs of substantia nigra compacta neurons (Nedergaard, 2004), is involved in spike frequency adaptation in adult Purkinje neurons (Sacco *et al.* 2003) and controls excitability and discharge dynamics of medial vestibular nucleus neurons (Pessia *et al.* 2008).

The effect of E-4031 in increasing MNTB firing is similar to that reported for blocking Kv1 channels, but differs from observations in cerebellar Purkinje and medial vestibular neurons, where ERG action reduces first spike latency (Sacco *et al.* 2003; Pessia *et al.* 2008). One key property of MNTB neurones is their fast action potentials (lasting less than 1 ms) which are much faster than APs in other principal cells in the CNS. This

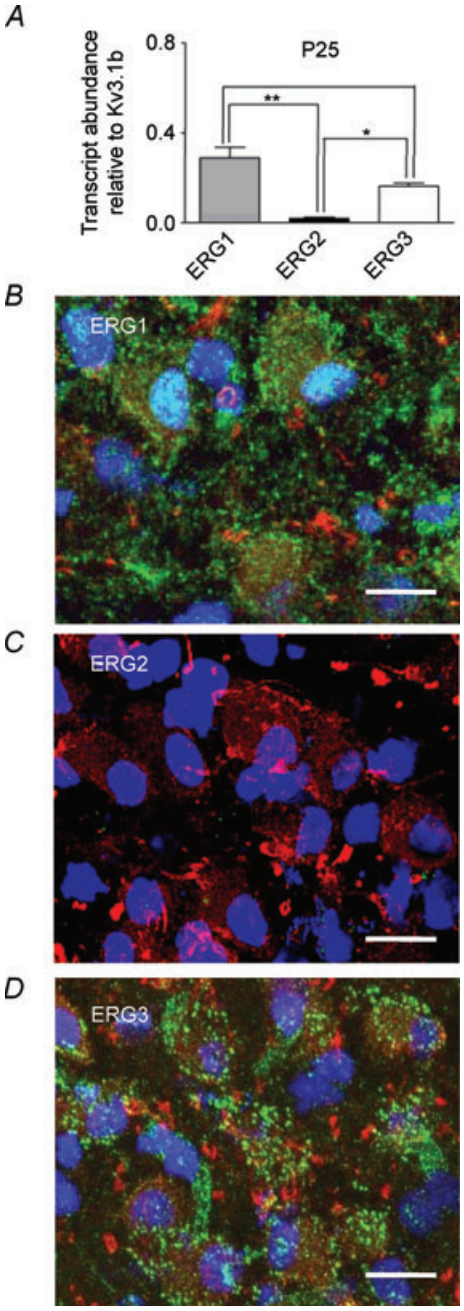

Figure 8. ERG1 and ERG3 are present in MNTB from P25 mice
A, QRT-PCR of ERG1, 2 and 3 mRNA expressed relative to Kv3.1b from P25 mice ($N = 3$, $n = 3$). ERG1 and ERG3 were present at significantly higher levels than ERG2 (one-way ANOVA with Bonferroni's correction, $^*P < 0.05$, $^{**}P < 0.01$). *B–D*, confocal projections of antibody staining for ERG1 (green) (*B*), ERG2 (green) (*C*) and ERG3 (green) co-labelled with Kv3.1b (red) and DAPI (blue) (*D*). Note the absence of ERG2 and the similar pattern of staining for ERG1 and 3 in P25 mice compared to P12 mice (Fig. 7*E*,*F*). Scale bar (20 μm) applies to all panels.

difference is important since longer action potentials will permit greater activation of a slow conductance such as ERG. However in a cell with fast APs, activation of voltage-gated channels with slow kinetics will accumulate during repetitive activity and thereby influence inter-spike potentials, as we demonstrated recently (Johnston *et al.* 2008*b*). ERG channels are predominantly localised on the soma and activate at relatively negative potentials, suggesting a role in controlling membrane excitability around threshold, analogous to Kv1 conductances. The increased conductance of ERG with raised $[K^+]_o$ may allow enhanced contribution of this conductance during periods of high auditory activity, when extracellular $[K^+]$ will rise and Kv1 channels inactivate. Interestingly, rat MNTB neurons have no detectable ERG but have much larger Kv1 currents than mouse (Dodson *et al.* 2002; Johnston *et al.* 2008*b*) suggesting that ERG expression in mouse may be one of several possible solutions to the main problem – that of regulating excitability around threshold voltages.

The presence of ERG within the auditory pathway raises interesting links with cardiovascular disease. There are more than 80 different mutations in the human *erg-1* gene which lead to long QT type 2 syndrome (LQT2) and acquired LQT involves blockade of ERG by pharmacological agents (Splawski *et al.* 2000). The familial form of LQT2 displays cardiac arrhythmic events triggered by sudden auditory stimuli (Wilde *et al.* 1999) or startle. These arrhythmic events are usually ascribed to sympathetic activation, but the pathway leading from auditory startle to sympathetic activation is likely to involve the brainstem startle reflex. Hence the present data suggest the hypothesis that ERG dysfunction in the brainstem could underlie the auditory trigger of LQT2 cardiac events, through auditory hyper-excitability and exaggerated startle reflexes.

References

Brew HM & Forsythe ID (1995). Two voltage-dependent K^+ conductances with complementary functions in postsynaptic integration at a central auditory synapse. *J Neurosci* **15**, 8011–8022.

Bustamante JO (2006). Current concepts in nuclear pore electrophysiology. *Can J Physiol Pharmacol* **84**, 347–365.

Cant NB & Casseday JH (1986). Projections from the anteroventral cochlear nucleus to the lateral and medial superior olive. *J Comp Neurol* **247**, 457–476.

Crociani O, Guasti L, Balzi M, Becchetti A, Wanke E, Olivotto M, Wymore RS & Arcangeli A (2003). Cell cycle-dependent expression of HERG1 and HERG1B isoforms in tumor cells. *J Biol Chem* **278**, 2947–2956.

Dodson PD, Barker MC & Forsythe ID (2002). Two heteromeric Kv1 potassium channels differentially regulate action potential firing. *J Neurosci* **22**, 6953–6961.

Dodson PD, Billups B, Rusznak Z, Szucs G, Barker MC & Forsythe ID (2003). Presynaptic rat Kv1.2 channels suppress synaptic terminal hyperexcitability following action potential invasion. *J Physiol* **550**, 27–33.

Gittelman JX & Tempel BL (2006). Kv1.1-containing channels are critical for temporal precision during spike initiation. *J Neurophysiol* **96**, 1203–1214.

Guasti L, Cilia E, Crociani O, Hofmann G, Polvani S, Becchetti A, Wanke E, Tempia F & Arcangeli A (2005). Expression pattern of the ether-a-go-go-related (ERG) family proteins in the adult mouse central nervous system: evidence for coassembly of different subunits. *J Comp Neurol* **491**, 157–174.

Hagendorf S, Fluegge D, Engelhardt C & Spehr M (2009). Homeostatic control of sensory output in basal vomeronasal neurons: activity-dependent expression of ether-a-go-go-related gene potassium channels. *J Neurosci* **29**, 206–221.

Han H, Wang J, Zhang Y, Long H, Wang H, Xu D & Wang Z (2004). HERG K channel conductance promotes H_2O_2-induced apoptosis in HEK293 cells: cellular mechanisms. *Cell Physiol Biochem* **14**, 121–134.

Hancox JC, Levi AJ & Witchel HJ (1998). Time course and voltage dependence of expressed HERG current compared with native "rapid" delayed rectifier K current during the ventricular action potential. *Pflugers Arch* **436**, 843–853.

Henkel CK & Gabriele ML (1999). Organization of the disynaptic pathway from the anteroventral cochlear nucleus to the lateral superior olivary nucleus in the ferret. *Anat Embryol (Berl)* **199**, 149–160.

Johnson JP Jr, Balser JR & Bennett PB (2001). A novel extracellular calcium sensing mechanism in voltage-gated potassium ion channels. *J Neurosci* **21**, 4143–4153.

Johnston J, Griffin SJ, Baker C & Forsythe ID (2008*a*). Kv4 (A-type) potassium currents in the mouse medial nucleus of the trapezoid body. *Eur J Neurosci* **27**, 1391–1399.

Johnston J, Griffin SJ, Baker C, Skrzypiec A, Chernova T & Forsythe ID (2008*b*). Initial segment Kv2.2 channels mediate a slow delayed rectifier and maintain high frequency action potential firing in medial nucleus of the trapezoid body neurons. *J Physiol* **586**, 3493–3509.

Joshi I & Wang LY (2002). Developmental profiles of glutamate receptors and synaptic transmission at a single synapse in the mouse auditory brainstem. *J Physiol* **540**, 861–873.

Mitcheson JS & Sanguinetti MC (1999). Biophysical properties and molecular basis of cardiac rapid and slow delayed rectifier potassium channels. *Cell Physiol Biochem* **9**, 201–216.

Nedergaard S (2004). A Ca^{2+}-independent slow afterhyperpolarization in substantia nigra compacta neurons. *Neuroscience* **125**, 841–852.

Ohya S, Horowitz B & Greenwood IA (2002). Functional and molecular identification of ERG channels in murine portal vein myocytes. *Am J Physiol Cell Physiol* **283**, C866–C877.

Pessia M, Servettini I, Panichi R, Guasti L, Grassi S, Arcangeli A, Wanke E & Pettorossi VE (2008). ERG voltage-gated K^+ channels regulate excitability and discharge dynamics of the medial vestibular nucleus neurons. *J Physiol* **586**, 4877–4890.

Postlethwaite M, Hennig MH, Steinert JR, Graham BP & Forsythe ID (2007). Acceleration of AMPA receptor kinetics underlies temperature-dependent changes in synaptic strength at the rat calyx of Held. *J Physiol* **579**, 69–84.

Roti EC, Myers CD, Ayers RA, Boatman DE, Delfosse SA, Chan EK, Ackerman MJ, January CT & Robertson GA (2002). Interaction with GM130 during HERG ion channel trafficking. Disruption by type 2 congenital long QT syndrome mutations. *J Biol Chem* **277**, 47779–47785.

Sacco T, Bruno A, Wanke E & Tempia F (2003). Functional roles of an ERG current isolated in cerebellar Purkinje neurons. *J Neurophysiol* **90**, 1817–1828.

Sanguinetti MC, Jiang C, Curran ME & Keating MT (1995). A mechanistic link between an inherited and an acquired cardiac arrhythmia: HERG encodes the IKr potassium channel. *Cell* **81**, 299–307.

Sanguinetti MC & Tristani-Firouzi M (2006). hERG potassium channels and cardiac arrhythmia. *Nature* **440**, 463–469.

Schneggenburger R & Forsythe ID (2006). The calyx of Held. *Cell Tissue Res* **326**, 311–337.

Shi W, Wymore RS, Wang HS, Pan Z, Cohen IS, McKinnon D & Dixon JE (1997). Identification of two nervous system-specific members of the *erg* potassium channel gene family. *J Neurosci* **17**, 9423–9432.

Smith PH, Joris PX, Carney LH & Yin TC (1991). Projections of physiologically characterized globular bushy cell axons from the cochlear nucleus of the cat. *J Comp Neurol* **304**, 387–407.

Smith PH, Joris PX & Yin TC (1998). Anatomy and physiology of principal cells of the medial nucleus of the trapezoid body (MNTB) of the cat. *J Neurophysiol* **79**, 3127–3142.

Splawski I, Shen J, Timothy KW, Lehmann MH, Priori S, Robinson JL, Moss AJ, Schwartz PJ, Towbin JA, Vincent GM & Keating MT (2000). Spectrum of mutations in long-QT syndrome genes: *KVLQT1*, *HERG*, *SCN5A*, *KCNE1*, and *KCNE2*. *Circulation* **102**, 1178–1185.

Steinert JR, Kopp-Scheinpflug C, Baker C, Challiss RA, Mistry R, Haustein MD, Griffin SJ, Tong H, Graham BP & Forsythe ID (2008). Nitric oxide is a volume transmitter regulating postsynaptic excitability at a glutamatergic synapse. *Neuron* **60**, 642–656.

Sturm P, Wimmers S, Schwarz JR & Bauer CK (2005). Extracellular potassium effects are conserved within the rat erg K^+ channel family. *J Physiol* **564**, 329–345.

Taschenberger H & von Geradorff H (2000). Fine-tuning an auditory synapse for speed and fidelity: developmental changes in presynaptic waveform, EPSC kinetics and synaptic plasticity. *J Neurosci* **20**, 9162–9173.

Wang LY, Gan L, Forsythe ID & Kaczmarek LK (1998). Contribution of the Kv3.1 potassium channel to high-frequency firing in mouse auditory neurons. *J Physiol* **509**, 183–194.

Wilde AA, Jongbloed RJ, Doevendans PA, Duren DR, Hauer RN, van Langen IM, van Tintelen JP, Smeets HJ, Meyer H & Geelen JL (1999). Auditory stimuli as a trigger for arrhythmic events differentiate HERG-related (LQTS2) patients from KVLQT1-related patients (LQTS1). *J Am Coll Cardiol* **33**, 327–332.

Zou A, Xu QP & Sanguinetti MC (1998). A mutation in the pore region of HERG K^+ channels expressed in *Xenopus* oocytes reduces rectification by shifting the voltage dependence of inactivation. *J Physiol* **509**, 129–137.

Acknowledgements

Thanks to Gail Robertson, University of Wisconsin for the gift of ERG1 antibody and to John Mitcheson, University of Leicester for helpful advice. This work was funded by the Medical Research Council.

Author's present address

R. M. Hardman: Department of Biology, University of Leicester, Leicester LE1 7RH, UK.